Type-II InAs/GaAsSb Quantum Dot Solar Cells With GaAs Interlayer

Dongyoung Kim, Sabina Hatch, Jiang Wu, Kimberly A. Sablon, Phu Lam, Pamela Jurczak, Mingchu Tang, William P. Gillin, and Huiyun Liu

Abstract—One of the primary challenges facing quantum dot (QD)-based intermediate band solar cells is the short lifetime of charge carriers ($\sim$1 ns). To investigate this, InAs QD/GaAs$_{1-x}$Sb$_x$ quantum well (QW) solar cells (SCs) with a 2-nm GaAs interlayer between the QDs and QW were fabricated for $x = 0$, 0.08, 0.14, and 0.17, respectively. Time-resolved photoluminescence measurements demonstrated prolonged carrier lifetimes up to 480 ns for the type-II SCs with $x \geq 14\%$. This improvement in carrier lifetime is assigned to the GaAs interlayer that reduces the wavefunction overlap between the electrons accumulated in the QDs and holes in the QW, and hence limits the possible emission pathways. External quantum efficiency measurements were performed to analyze the SC performance. An order of magnitude improvement was observed in the QD region (900–1200 nm) for the type-II SCs and is linked to the prolonged carrier lifetime.

Index Terms—Intermediate band solar cells (IBSCs), molecular beam epitaxy, quantum dot (QD) solar cells.

I. Introduction

INTERMEDIATE band solar cells (IBSCs) have the potential to exceed the Shockley–Queisser limit and achieve power conversion efficiency up to 63% [1]. Quantum dots (QDs) are used to form an intermediate band (IB) within a single-junction solar cell (SC) due to their three-dimensional (3-D) confinement and tunable bandgap. However, the use of QDs in III–V SCs has proven to be difficult in many aspects. First, the thermal coupling between the IB and conduction band (CB) removes the need for two-photon excitation [2]–[4]. Thermal coupling occurs when carriers are able to transition between the IB and CB via thermal excitation and relaxation, which

consequently, lowers the open-circuit voltage (V_{OC}) [5], [6]. Second, the strain accumulation that originates from the lattice mismatch between InAs QDs and GaAs can lead to the formation of dislocations [7], [8], and hence inhibit the growth of numerous QD layers that are needed to maximize photon absorption [7]–[10]. Furthermore, the type-I band alignment formed by InAs/GaAs QD SCs allows efficient radiative recombination, resulting in short carrier lifetimes ($\sim$1 ns). This significantly reduces the probability of two-photon absorption occurring [11].

It has been demonstrated that a higher crystal quality and QD density can be achieved using GaAsSb as a strain reducing layer on InAs QDs [11]–[13]. In this way, optical properties of the QD region can be enhanced and nonradiative recombination can be reduced. Also, GaAsSb enables the formation of a type-II band alignment for InAs/GaAsSb QD system. Unlike type-I band alignment, where electrons and holes are confined in the same spatial region, a type-II band alignment spatially separates the photo-excited charge carriers and prolongs the carrier lifetime [14]–[16]. Valence band offset (VBO) between the InAs QDs and GaAs$_{1-x}$Sb$_x$ QW depends on the Sb composition; the crossover between type-I and type-II band alignment is reported to occur when $x = 0.12$ [17]–[19]. Although the prolonged carrier lifetime increases the probability for two-photon absorption, the improvement in quantum efficiency could be limited by the change in hole dynamics across the active region [20].

We previously demonstrated enhanced type-II characteristics in the InAs-QD/GaAs$_{0.83}$Sb$_{0.17}$-QW hybrid SC when a GaAs interlayer was inserted between the InAs QDs and GaAsSb QW [20]. A 23% improvement in power conversion efficiency was observed compared with the structure without the GaAs interlayer. This behavior was attributed to a reduction in VB confinement in the GaAsSb QW, which lowered the potential barrier for hole transport across the active region. To further examine this phenomenon, hybrid InAs-QD/GaAs$_{1-x}$Sb$_x$-QW SCs with a GaAs interlayer with $x = 0, 0.08$, 0.14, and 0.17 are studied. Power-dependent, temperature-dependent, and time-resolved photoluminescence (PL) measurements are used to investigate the radiative emission pathways and identify the presence of type-II band alignment. Current density–voltage (*J–V*) and external quantum efficiency (EQE) measurements are used to characterize the SC performance and demonstrate the benefit of introducing a GaAs interlayer to the type-II InAs-QD/GaAsSb-QW SCs.
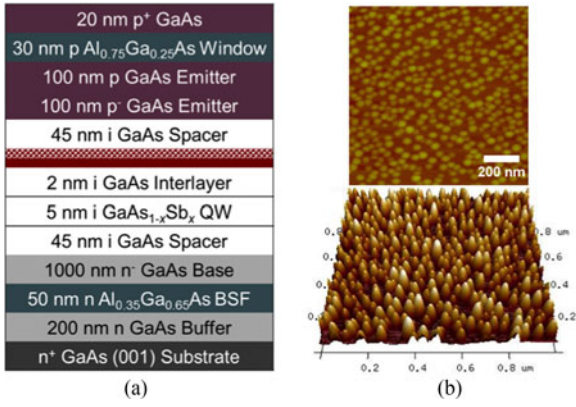
Fig. 1. (a) Structure of the hybrid InAs-QD/GaAs$_{1-x}$Sb$_x$-QW SCs ($x = 0, 0.08, 0.14,$ and 0.17). (b) AFM images of InAs QDs grown on 2 nm GaAs in 2-D (top) and 3-D (bottom).

II. EXPERIMENTAL

Four hybrid InAs-QD/GaAsSb-QW SC samples were grown by a solid-source molecular beam epitaxy on n$^+$-GaAs (100) substrates. As shown in Fig. 1(a), all SCs are grown with the same p-i-n structure that consists of a 200-nm GaAs buffer layer with Si doping density of 2×10^{18} cm^{-3}, 50 nm Al$_{0.35}$Ga$_{0.65}$As back surface field layer with Si doping density of 2×10^{18} cm^{-3}, 1000 nm GaAs base with Si doping density of 2×10^{17} cm^{-3}, 100 nm GaAs emitter with Be doping density of 1×10^{18} cm^{-3}, 100 nm GaAs emitter with Be doping density of 5×10^{18} cm^{-3}, 30 nm Al$_{0.79}$Ga$_{0.21}$As window layer with Be doping density of 5×10^{18} cm^{-3}, and 20 nm GaAs contact layer with Be doping density of 1×10^{19} cm^{-3}. The intrinsic region of the SCs consists of 20 stacks of hybrid InAs-QDs/GaAs$_{1-x}$Sb$_x$QWs separated by a 45 nm GaAs spacer. To form hybrid InAs-QD/GaAsSb-QW structure, a 2 nm GaAs interlayer is inserted between 2.1-MLs InAs QDs and 5-nm GaAs$_{1-x}$Sb$_x$-QW. The QDs are grown by the Stranski–Krastanov mode at substrate temperature of ∼500 °C measured by a pyrometer. A Veeco Nanoscope V atomic force microscope (AFM) was used to characterize the morphology of uncapped InAs QDs on GaAs interlayer, as shown in Fig. 1(b). The average diameter of the QDs was measured to be ∼40 nm, with an average height of ∼6 nm. No large defected dots were observed in large AFM images, indicating a high structural quality [21]. The QD density per layer was estimated to be ∼4.3×10^{10} cm^{-2}. Increasing the Sb composition in the GaAs$_{1-x}$Sb$_x$ QW did not have significant influence on the shape, size, and the density of the QDs, unlike Sb mediated QD growth [22]. GaAs spacer layers grown at a high growth temperature (580 °C) are applied during the growth of QDs to suppress the formation of dislocations [7], [10], [23]. In this paper, four Sb compositions ($x = 0, 0.08, 0.14,$ and 0.17) are investigated for the GaAs$_{1-x}$Sb$_x$ QW.

For device fabrication, an Au–Zn alloy (95% Au, 5% Zn) is thermally evaporated to form a (∼220 nm thick) grid-pattern p-type electrode using a metal shadow mask. The masked area is ∼0.13 cm^2. For the n-type electrode, Ni (10 nm), Au–Ge (12%) (100 nm), Ni (30 nm), and Au (160 nm) are thermally evaporated onto the entire back surface, and rapidly thermally annealed in forming gas at 400 °C for 60 s. No antireflective coating or surface passivation is applied to these SCs. A typical SC has a device area of 0.5 cm^2.

J–V measurements are performed under one-sun (AM 1.5G) illumination using a LOT calibrated solar simulator with a Xeon lamp. A 4-point probe station is used to connect the devices to a Keithly 2400 sourcemeter that outputs the data to Photor 3.1 software. Photocurrent measurements is obtained with a halogen lamp chopped to a frequency of 188 Hz through a Newport monochromator; a 4-point probe in connection with a lock-in amplifier is used to collect data. The monochromatic beam is calibrated using a Silicon photodiode and the data analyzed with Tracer 3.2 software to produce the EQE. Temperature-dependent and power-dependent PL spectra are obtained using continuous-wave PL measurements performed using 532 nm excitation from a diode pumped solid-state laser. A cryostat is used to control the sample temperature between 10 and 300 K.

Transient photoluminescence (TRPL) is examined using a 6 ns pulse at 505 nm from a Continuum Panther optical parametric oscillator (OPO) pumped with a Surelite-I laser. The sample is held at 80 K in an Oxford Instruments Optistat continuous flow cryostat and the luminescence is dispersed in a Triax 550 spectrometer with a 600-lines/mm grating Blazed at 1 μm. The luminescence is detected with a Hamamatsu R5509-72 photomultiplier and recorded using a LeCroy Waverunner-2 Oscilloscope.

III. RESULTS AND DISCUSSION

Fig. 2(a) shows the temperature-dependent PL spectra (20–300 K) of the hybrid InAs-QD/GaAs$_{1-x}$Sb$_x$-QW SCs. At 300 K, the PL intensity for $x = 0.08$ to 0.17 drops by two orders of magnitude compared with $x = 0$. A reduction in QD peak intensity is an indicator of type-II band alignment due to the lower photon absorption efficiency. This behavior is therefore expected for samples with $x = 0.14$ and 0.17. Two peaks are observed for $x = 0.14$ and 0.17. At temperatures above 140 K, the intensity of the high-energy peak exceeds that of the low-energy peak. This is unusual because carriers are expected to easily transition to lower energy states at higher temperatures. As the temperature drops below 140 K, the low energy peak starts to dominate. This indicates a preferred emission pathway through a higher energy state at higher temperatures, which is inhibited at low temperatures.

Fig. 2(b) shows the log-scale power-dependent PL spectra of the hybrid solar cells measured at 10 K. The QD peak emission for $x = 0$ spans a wide range of wavelengths (900–1100 nm), which indicates a large size distribution of QDs is present. The GaAs peak can clearly be identified at ∼830 nm. The GaAs peak is an order of magnitude higher for samples with Sb present. This can be linked to the conduction band offset (CBO) formed between the GaAs and GaAsSb QW. At 10 K, the electrons in the GaAs CB are inhibited by the CBO from transitioning to lower energy states in the QDs, thereby increasing GaAs peak emission. The onset of the QD peak emission is shown to redshift with increasing Sb composition from 900 to 1000 nm. This is attributed to the increasing VBO between the QD and the QW for increasing Sb composition.
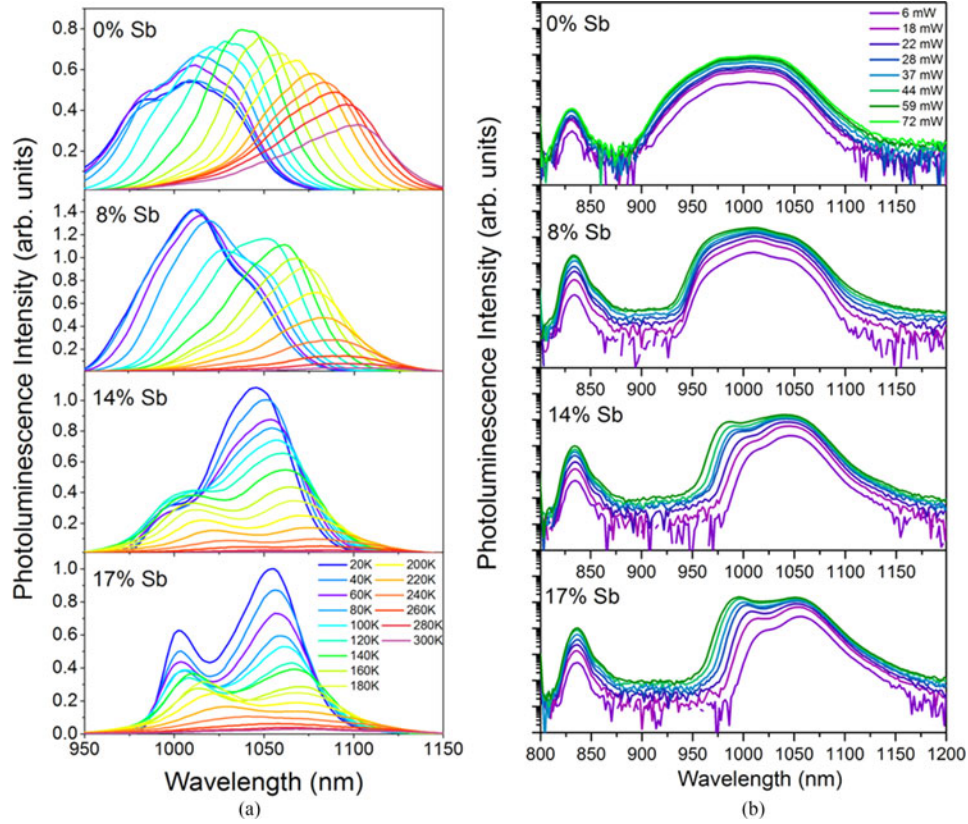
Fig. 2. Photoluminescence spectra of hybrid InAs-QD/GaAs$_{1-x}$Sb$_x$-QW SCs ($x = 0, 0.08$, 0.14, and 0.17) showing (a) linear-scale temperature-dependent measurements at 37 mW laser excitation, and (b) semi-log scale laser excitation power-dependent measurements at 10 K.

Fig. 3(a) shows the decay time of the hybrid InAs-QD/GaAs$_{1-x}$Sb$_x$ –QW SCs measured at 1050 nm emission. Both $x = 0$ and 0.08 show decays times comparable to that of the laser (∼3 ns), confirming type-I behavior. Whereas significantly prolonged carrier lifetimes approaching 480 ns were measured for the samples with $x = 0.14$ and $x = 0.17$ [24]. This exceeds previously reported type-II carrier lifetimes by almost two-and-half times. A double exponential decay fitting

$$y = y_0 + A_1 e^{-\frac{t}{\tau_1}} + A_2 e^{-\frac{t}{\tau_2}}$$

is used to calculate the carrier lifetimes across the 900–1100 nm spectra. Fig. 3(b) shows the type-II SCs have two distinct carrier lifetimes, 5–15 ns and 100–500 ns. Fig. 3(c) shows the absolute PL intensity plotted against the emission wavelength to determine the peak contribution for each decay time. The fast decay (τ_1) and slow decay (τ_2) times are represented by square and circle symbols, respectively. Fig. 3(c) shows the sample with $x = 0.14$ (green) has peaks at $\tau_1 \sim 1050$ nm and $\tau_2 \sim 1055$ nm, $x = 0.17$ has two peaks at $\tau_1 \sim 990$ and 1060 nm, and one at $\tau_2 \sim 1080$ nm. This indicates multiple decay pathways. The separation of charge carriers gives rise to the band bending in the GaAsSb-QW. This is predicted to create a potential well (H_0) close to the QW/GaAs-interlayer interface, and a second energy state (H_1) across the QW region. The QD electron ground state E_0 has a narrower wavefunction than the excited state E_1 due to the deeper confinement. The overlap of these electron-hole wavefunctions determines the possible emission pathways and explains the two different decay times. Due to the spatial separation of charge carriers in the type-II SCs, the selection rules start to break down and allow new emission pathways to exist [19], [25]. However, the new emission pathways, E_0H_1 and E_1H_0, are expected to be weaker.

By examining the e$^-$/h$^+$ wavefunctions overlap, the shorter carrier lifetime, τ_1, is assigned to E_1H_0 and E_1H_1, while the prolonged carrier lifetime, τ_2, originates from E_0H_1 and E_0H_0 emission. H_1 have greater sensitivity to band bending than H_0 due to the electric field accumulating holes close to the GaAsSb-QW/GaAs interlayer interface. This also explains the two peak energies for $x = 0.14$ and 0.17 that do not shift with increasing laser excitation power, E_0H_0 and E_1H_0. This is further evidenced by the temperature-dependent PL that shows for $T > 140$ K, the excited state QD emission is more favorable than the ground state. However, below 140 K, electrons can no longer thermally escape to E_1 and E_0 emission starts to dominate. In addition, previously reported power-dependent TRPL for a similar structure shows that carrier lifetime increases with decreasing excitation intensity [24]. This supports the suggested theory, as fewer carriers will be promoted to the higher energy states that lead to the faster decay transitions. The GaAs interlayer, therefore, serves to further restrict the e$^-$/h$^+$ wavefunction overlap and prolong the carrier lifetime beyond that of InAs-QD/GaAsSb-QW SCs without the GaAs interlayer.
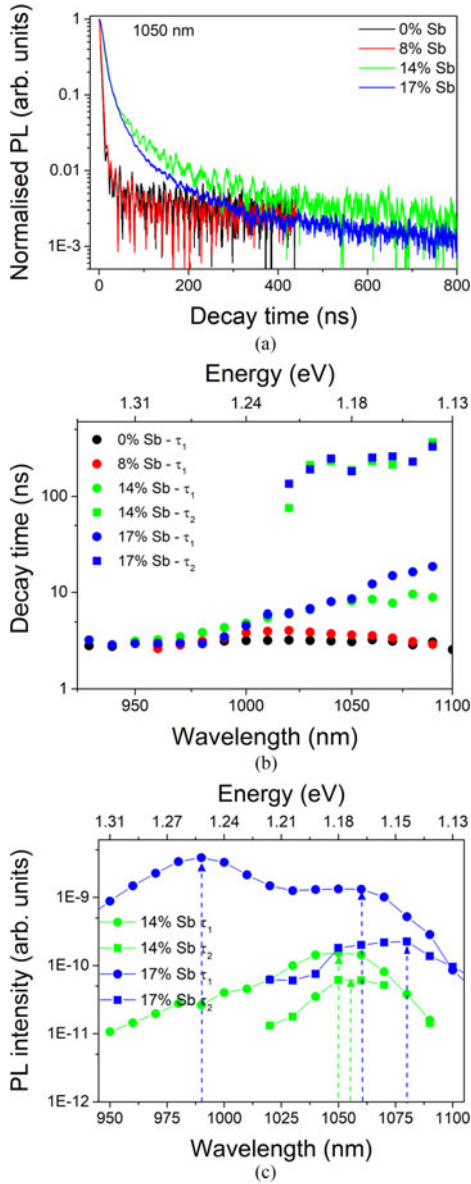
Fig. 4. Current-density versus voltage plot of InAs QDs/GaAs interlayer/GaAs$_{1-x}$Sb$_x$ QW solar cells for $x = 0, 0.08$, 0.14 and 0.17. Measurements were conducted under one sun with global AM 1.5 illumination at room temperature.

TABLE I
SHORT-CIRCUIT CURRENT DENSITY (J_{SC}), OPEN-CIRCUIT
VOLTAGE (V_{OC}), FILL FACTOR (FF), AND EFFICIENCY (η)
DERIVED FROM THE J–V PLOT IN FIG. 4

Device	J_{SC} (mA cm^{-2})	V_{OC} (V)	FF (%)	η (%)
0 Sb	17.6	0.86	75.4	11.5
0.08 Sb	17.7	0.74	65.5	8.6
0.14 Sb	18.0	0.70	71.3	9.0
0.17 Sb	18.0	0.68	71.4	8.7

Fig. 3. Time-resolved PL spectra of hybrid InAs-QD/GaAs$_{1-x}$Sb$_x$-QW SCs ($x = 0, 0.08$, 0.14, and 0.17) at 80 K. (a) Normalized PL intensity versus decay time at 1050 nm emission. (b) Carrier decay time versus emission wavelength. (c) Absolution PL intensity contributions of the different decay components for $x = 0.14$ and 0.17.

J–V measurements were performed on the hybrid InAs-QDs/GaAs$_{1-x}$Sb$_x$-QW SCs with GaAs interlayer as shown in Fig. 4. The short-circuit current density (J_{SC}), open-circuit voltage (V_{OC}), fill factor (FF), and efficiency (η) are derived from the J–V plot and presented in Table I. The earlier study showed a significant reduction in J_{SC} with increasing Sb composition [20]. It is clear that by inserting a GaAs interlayer into the hybrid SC structure, a high J_{SC} of 18.0 mA cm^{-2} can be achieved for the $x = 0.14$ and 0.17 SCs. Although this J_{SC} is 0.4 mA cm^{-2} higher than the reference $x = 0$ type-I QDSC, the overall efficiency is 2.5% lower due to the drop in V_{OC}.

As with the previous study, the drop in V_{OC} is prevalent as shown in Fig. 4. The V_{OC} is primarily governed by the bandgap
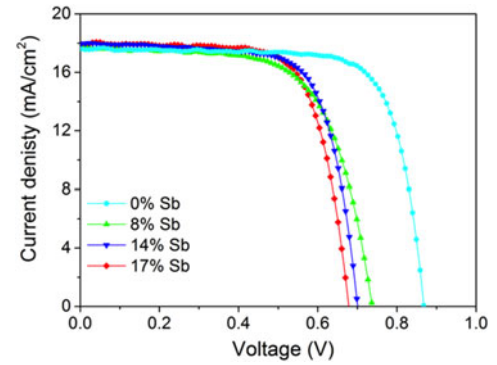
energy and recombination current of the SC. A difference of 0.18 V between $x = 0$ and 0.17 is too large to be solely due to the reduction in bandgap energy. This is supported by the significant drop in V_{OC} observed for $x = 0.08$ which has type-I band alignment and has the same energy as that of $x = 0$. Therefore, as indicated by the reduction in temperature-dependent PL intensity in Fig. 2(a), the nonradiative recombination centers play a significant role in limiting the overall device efficiency. This can be assigned to a high density of strain-induced dislocations that reduce minority carrier lifetime and diffusion length. Postgrowth rapid thermal annealing to remove the point defects, or introducing Si doping to the QDs can potentially recover the V_{OC} [26]–[28].

The EQE spectra in Fig. 5 demonstrate the photocurrent generated between 350 and 1100 nm at zero-bias and is directly related to the J_{SC} measured in Fig. 4. In the absence of an antireflective coating and passivation layer, the EQE shows a limited photoresponse for higher photon energies (350–500 nm) that are collected close to the surface. Between 700 and 900 nm, the EQE for type-I ($x < 0.14$) and type-II ($x \geq 0.14$) band alignment can be clearly distinguished. The insertion of the GaAs interlayer has shown that it can greatly improve the EQE in this region by increasing the QW confinement and, therefore, lowering the potential barrier for holes to transition to the VB. However, the introduction of strained GaAsSb layers is likely to degrade the material quality, which leads to increased nonradiative recombination and lower EQE observed between 700 and 900 nm. It is worth noting that IBSCs are designed to operate under concentrated illumination (i.e., 500 suns), where a high density of charge carriers will be generated. Hence, the
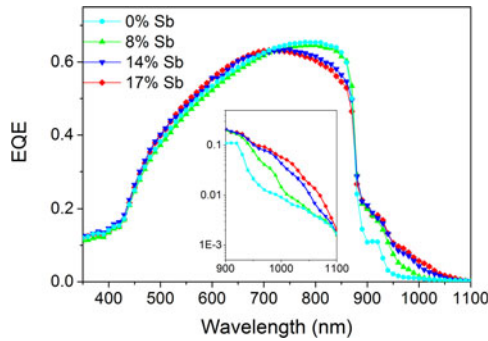
Fig. 5. Linear-scale external quantum efficiency spectra of a GaAs reference solar cell and InAs QDs/GaAs interlayer/GaAs$_{1-x}$Sb$_x$ QW solar cells, where $x = 0, 0.08, 0.14$ and 0.17. The inset shows an enlarged semilog scale plot that corresponds to the QD region.

restrictions to hole transport across the QW will be minimized as the hole concentration in the QW increases and further lowers the VB potential barrier.

The inset of Fig. 5 shows the semilog scale plot of the WL and QD region. In the QD region (950–1100 nm), an order of magnitude improvement in EQE can be observed between the $x = 0$ and 0.17. This can be credited to both the significantly prolonged carrier lifetime associated with the type-II band alignment, and the improved hole transport across the active region generated by the GaAs interlayer.

IV. CONCLUSION

In conclusion, hybrid InAs-QD/GaAs$_{1-x}$Sb$_x$-QW SCs ($x = 0, 0.08, 0.14$, and 0.17) with a GaAs interlayer were studied. Type-II band alignment was demonstrated using power-dependent PL measurements for the samples with $x = 0.14$ and $x = 0.17$ and prolonged carrier lifetime up to 480 ns was shown by transient PL measurements. The prolonged lifetime was attributed to the GaAs interlayer that served to further reduce the e$^-$/h$^+$ wavefunction overlap of the type-II structure. Both $x = 0.14$ and 0.17 exhibited a high J_{SC} of $18.0 \, \text{mA} \, \text{cm}^{-2}$ with efficiency of 9.0% and 8.7%, respectively. EQE measurements confirmed the improvement in J_{SC} is due to the increased photocurrent contribution from the QD region. This is linked to the prolonged lifetime associated with the type-II band alignment and the insertion of the GaAs interlayer. This provides a mean to overcome the challenges related to the short carrier lifetime of type-I QD-IBSCs.

REFERENCES

[1] A. Luque and A. Martí, "Increasing the efficiency of ideal solar cells by photon induced transitions at intermediate levels," *Phys. Rev. Lett.*, vol. 78, no. 26, pp. 5014–5017, Jun. 1997.

[2] S. Sanguinetti *et al.*, "Carrier thermal escape and retrapping in self-assembled quantum dots," *Phys. Rev. B*, vol. 60, no. 11, pp. 8276–8283, Sep. 1999.

[3] E. Antolín *et al.*, "Reducing carrier escape in the InAs/GaAs quantum dot intermediate band solar cell," *J. Appl. Phys.*, vol. 108, no. 6, Sep. 2010, Art. no. 064513.

[4] A. Luque and A. Martí, "The intermediate band solar cell: Progress toward the realization of an attractive concept," *Adv. Mater.*, vol. 22, no. 2, pp. 160–174, Nov. 2010.

[5] C. G. Bailey, D. V. Forbes, R. P. Raffaelle, and S. M. Hubbard, "Near 1 V open circuit voltage InAs/GaAs quantum dot solar cells," *Appl. Phys. Lett.*, vol. 98, no. 16, Apr. 2011, Art. no. 163105.

[6] A. Mellor, A. Luque, I. Tobías, and A. Martí, "Realistic detailed balance study of the quantum efficiency of quantum dot solar cells," *Adv. Funct. Mater.*, vol. 24, no. 3, pp. 339–345, Jan. 2014.

[7] F. K. Tutu *et al.*, "Improved performance of multilayer InAs/GaAs quantum-dot solar cells using a high-growth-temperature GaAs spacer layer," *J. Appl. Phys.*, vol. 111, no. 4, Feb. 2012, Art. no. 046101.

[8] A. Martí *et al.*, "Emitter degradation in quantum dot intermediate band solar cells," *Appl. Phys. Lett.*, vol. 90, no. 23, Jun. 2007, Art. no. 233510.

[9] T. Sugaya *et al.*, "Multi-stacked quantum dot solar cells fabricated by intermittent deposition of InGaAs," *Sol. Energy Mater. Sol. Cells*, vol. 95, no. 1, pp. 163–166, Jan. 2011.

[10] H. Y. Liu *et al.*, "Improved performance of 1.3 μm multilayer InAs quantum-dot lasers using a high-growth-temperature GaAs spacer layer," *Appl. Phys. Lett.*, vol. 85, no. 5, pp. 704–706, Aug. 2004.

[11] K.-Y. Ban *et al.*, "Controllability of the subband occupation of InAs quantum dots on a delta-doped GaAsSb barrier," *J. Appl. Phys.*, vol. 109, no. 1, Jan. 2011, Art. no. 014312.

[12] W.-S. Liu *et al.*, "High optical property vertically aligned InAs quantum dot structures with GaAsSb overgrown layers," *J. Cryst. Growth*, vol. 323, no. 1, pp. 164–166, May 2011.

[13] S. P. Bremner, K.-Y. Ban, N. N. Faleev, C. B. Honsberg, and D. J. Smith, "Impact of stress relaxation in GaAsSb cladding layers on quantum dot creation in InAs/GaAsSb structures grown on GaAs (001)," *J. Appl. Phys.*, vol. 114, no. 10, Sep. 2013, Art. no. 103511.

[14] W.-S. Liu, Y.-T. Wang, W.-Y. Qiu, and C. Fang, "Carrier dynamics of a Type-II vertically aligned InAs quantum dot structure with a GaAsSb strain-reducing layer," *Appl. Phys. Exp.*, vol. 6, no. 8, Aug. 2013, Art. no. 085001.

[15] S. Tomić, "Effect of Sb induced type II alignment on dynamical processes in InAs/GaAs/GaAsSb quantum dots: Implication to solar cell design," *Appl. Phys. Lett.*, vol. 103, no. 7, Aug. 2013, Art. no. 072112.

[16] R. B. Laghumavarapu *et al.*, "GaSb/InGaAs quantum dot–well hybrid structure active regions in solar cells," *Sol. Energy Mater. Sol. Cells*, vol. 114, pp. 165–171, Jul. 2013.

[17] H. Y. Liu *et al.*, "Long-wavelength light emission and lasing from InAs/GaAs quantum dots covered by a GaAsSb strain-reducing layer," *Appl. Phys. Lett.*, vol. 86, no. 14, Apr. 2005, Art. no. 143108.

[18] K.-Y. Ban, D. Kuciauskas, S. P. Bremnerand, and C. B. Honsberg, "Determination of a Sb composition in InAs/GaAsSb for negligible valence band offset," in *Proc. 2010 35th IEEE Photovolt. Spec. Conf.*, 2010, pp. 003306–003309.

[19] K.-Y. Ban, D. Kuciauskas, S. P. Bremner, and C. B. Honsberg, "Observation of band alignment transition in InAs/GaAsSb quantum dots by photoluminescence," *J. Appl. Phys.*, vol. 111, no. 10, May 2012, Art. no. 104302.

[20] S. Hatch *et al.*, "InAs/GaAsSb quantum dot solar cells," *Opt. Express*, vol. 22, no. S3, pp. A679–A685, May 2014.

[21] H. Y. Liu *et al.*, "p-doped 1.3 μm InAs/GaAs quantum-dot laser with a low threshold current density and high differential efficiency," *Appl. Phys. Lett.*, vol. 89, no. 7, Aug. 2006, Art. no. 073113.

[22] F. K. Tutu *et al.*, "Antimony mediated growth of high-density InAs quantum dots for photovoltaic cells," *Appl. Phys. Lett.*, vol. 103, no. 4, Jul. 2013, Art. no. 043901.

[23] H. Y. Liu *et al.*, "Influences of the spacer layer growth temperature on multilayer InAs/GaAs quantum dot structures," *J. Appl. Phys.*, vol. 96, no. 4, pp. 1988–1992, Aug. 2004.

[24] K. Nishikawa *et al.*, "Extremely long carrier lifetime over 200 ns in GaAs wall-inserted type II InAs quantum dots," *Appl. Phys. Lett.*, vol. 100, no. 11, Mar. 2012, Art. no. 113105.

[25] C. Y. Jin *et al.*, "Optical transitions in type-II InAs/GaAs quantum dots covered by a GaAsSb strain-reducing layer," *Appl. Phys. Lett.*, vol. 91, no. 2, Jul. 2007, Art. no. 021102.

[26] P. Lam *et al.*, "The effect of rapid thermal annealing on InAs/GaAs quantum dot solar cells," *IET Optoelectron.*, vol. 9, no. 2, pp. 65–68, 2014.

[27] P. Lam *et al.*, "Voltage recovery in charged InAs/GaAs quantum dot solar cells," *Nano Energy*, vol. 6, pp. 159–166, May 2014.

[28] D. Kim *et al.*, "Si-doped InAs/GaAs quantum-dot solar cell with AlAs cap layers," *IEEE J. Photovolt.*, vol. 6, no. 4, pp. 906–911, Jul. 2016.